Journal of Materials Chemistry A

ROYAL SOCIETY OF CHEMISTRY

COMMUNICATION

View Article Online
View Journal | View Issue

Check for updates

Cite this: J. Mater. Chem. A, 2023, 11, 1108

Received 17th October 2022
Accepted 14th December 2022

DOI: 10.1039/d2ta08127j

rsc.li/materials-a

Published on 15 2565. Downloaded on 25/7/2567 1:05:24.

Waste PET upcycling to conductive carbon-based composite through laser-assisted carbonization of UiO-66†

Dmitry Kogolev, ‡[a] Oleg Semyonov, ‡[a] Nadezhda Metalnikova,[a] Maxim Fatkullin,[a] Raul D. Rodriguez,[a] Petr Slepicka,[b] Yusuke Yamauchi,[cd] Olga Guselnikova,[ad] Rabah Boukherroub[e] and Pavel S. Postnikov *[ab]

The upcycling of waste polymers into novel materials with high added value is a vital task for modern chemical engineering. Here, we propose diversifying waste polyethylene terephthalate (PET) upcycling to materials with enhanced photothermal properties by laser-assisted carbonization of surface-grown UiO-66. The UiO-66 homogenous layer was formed using a solvo-thermal procedure on the surface of recycled PET sheets. The treatment by a 405 nm laser system allowed the formation of a carbonaceous layer with enhanced electrical conductivity and photothermal properties due to the presence of zirconium carbide and graphene. The developed approach opens new perspectives in the application of upcycled PET-based materials.

The fast-growing production of polymer materials has led to crucial problems owing to environmental contamination by plastic waste.[1,2] Polyethylene terephthalate (PET) is a widespread polyether that significantly contributes to the polymer waste challenge.[3] For instance, waste PET has been transformed into adsorbents for environmental contaminants,[4] smart textiles,[5] and catalysts.[6] However, the high functionality of PET could facilitate further diversification of applications of waste PET-derived materials.

The main strategy of functional upcycling is the transformation of the outer polymer layer with conservation of the bulk polymer substrates.[7,8] PET is hydrolysed relatively easily by the formation of free carboxylic groups, which are excellent anchor moieties. These carboxylic groups are involved in the surface-assisted growth of metal–organic framework (MOF) layers on the surface of hydrolysed PET.[9,10] Here, PET was used as the support and feedstock for MOFs synthesis.[11] This allows for the design of a wide range of materials to remove the organic pollutants from the environment.[6,10] However, MOF applications are not limited to adsorption and catalysis. An alternative pathway for upcycled PET@MOF-derived materials is carbonisation under elevated temperatures in an inert atmosphere with the formation of carbon-based materials.[12–17] Functional carbonised materials are finding applications as energy-related tools, such as supercapacitors,[18,19] photothermal,[20,21] and photovoltaic devices.[22,23]

Carbonisation is traditionally performed by thermal annealing, which requires harsh conditions and is energy-intensive.[24,25] Sufficient progress in this field has been achieved by implementing a laser beam as the source of energy for the carbonisation of thin-layered MOF powders.[26–29]

Laser-induced carbonisation allows the conversion of thin-layered MOF powders to metal nanoparticles,[26] graphene–metal monolites,[27] or carbon-based materials with incorporated metal nanostructures.[28–31] Thus, this method has considerable potential for the design of novel materials with improved properties using MOFs as feedstock in a mild, scalable and energy-efficient manner.

Laser annealing is a fascinating option for the treatment of polymer-supported thin-layered MOFs. In such a case, the carbonisation process should be accompanied by partial melting of the polymer matrix with the formation of a durable composite, similar to previous findings.[32,33] Moreover, the formation of a thin carbon film on the polymer surface improves the performance of the resulting material in photothermal applications because of the insulating properties of the polymer support and absence of heat dissipation.[34,35] In addition, owing to its flexibility and durability, PET can be applied as a support for bendable electronic devices in flexible circuits, photo, pressure, and wearable sensors,[36–40] such as skin

[a]Research School of Chemistry and Applied Biomedical Sciences, Tomsk Polytechnic University, Tomsk 6340034, Russian Federation. E-mail: postnikov@tpu.ru
[b]Department of Solid State Engineering, University of Chemistry and Technology, 16628 Prague, Czech Republic
[c]Australian Institute for Bioengineering and Nanotechnology (AIBN), The University of Queensland, Brisbane, QLD 4072, Australia
[d]JST-ERATO Yamauchi Materials Space-Tectonics Project and International Center for Materials Nanoarchitectonics (WPI-MANA), National Institute for Materials Science (NIMS), Tsukuba, Ibaraki 305-0044, Japan
[e]Univ. Lille, CNRS, Centrale Lille, Univ. Polytechnique Hauts-de-France, IEMN, UMR CNRS 8520, F-59000 Lille, France

† Electronic supplementary information (ESI) available. See DOI: https://doi.org/10.1039/d2ta08127j

‡ Equal contributors.

This journal is © The Royal Society of Chemistry 2023

Published on 15 2565. Downloaded on 25/7/2567 1:05:24.

bioelectrodes,[41] breath/gas sensors, flexors, and skin conductance sensors.[42] The development of such materials is promising and critical for microelectronic technologies, wearable devices, and the internet of things, which are based on economic effectiveness, scalability, and mechanical and chemical stability.[43,44]

In this study, we propose a novel approach for the functional upcycling of PET to composite carbon-based materials *via* the preliminary growth of UiO-66 crystals on the surface followed by laser-induced carbonisation (Fig. 1). The resulting material PET@LB-UiO-66 (LB = laser-burned) represents a composite with a graphene-like material fused in the PET matrix with enhanced mechanical stability and high surface conductivity of 10.4 ± 3.1 Ω per square. Moreover, the PET@LB-UiO-66 has a considerable photothermal response, reaching 71 °C under illumination by 660 nm light-emitting diode (LED) with a power density of 0.036 kW m^{-2} after 100 s.

Transparent PET sheets made from recycled plastic were purchased from a hardware store as a starting material. We started our investigation by adopting a previously reported procedure for UiO-66 growth on recycled PET sheets (Section 2, ESI†).[10] The process included two stages: (i) hydrolysis and (ii) growth of the UiO-66 layer. In the first stage, we optimised the temperature and treatment with concentrated H_2SO_4 for the hydrolysis step and monitored the characteristic νO–H stretching vibration band by Fourier-transform infrared (FTIR) spectroscopy. The highest intensity of the νO–H band, corresponding to the highest hydrolysis degree, was achieved by treatment with concentrated H_2SO_4 for 5 min at 75 °C (Fig. S1 and S2, ESI†). Moreover, such conditions allow the PET sheet to remain in shape without significant degradation or deformation during the hydrolysis process, which is extremely important for applications. After hydrolysis, a polycrystalline UiO-66 layer was formed (Fig. S3 and S4† and a brief description of the method and characterisation of the resulted material are given in Section 3, ESI†).[10] For UiO-66 growth, the sheets were loaded with $ZrCl_4$ and terephthalic acid prepared from waste PET bottles.[45]

Scanning electron microscopy (SEM) analysis (Fig. S3D–F, ESI†) revealed that the prepared PET@UiO-66 was characterised by a homogeneously distributed polycrystalline layer of UiO-66, which is favourable for further laser treatment. The homogeneity of the UiO-66 coating is crucial for the further uniformity of the laser-treated carbon layers. Previously, surface-assisted MOF treatment required the addition of binders for MOF powder[46] or preliminary MOF carbonisation and deposition on the substrate.[47,48] The direct growth of UiO-66 guarantees the homogeneity and stability of the functional layer after the laser treatment.

To determine the appropriate wavelength, we performed an ultraviolet-visible (UV-vis) study of the prepared composite, which showed an absorbance maximum at 375 nm (Fig. 2A). Such an absorbance peak was not observed in pristine or hydrolysed PET. This indicates the potential for selective carbonisation of the MOF layer without considerable involvement of the bulk PET (Fig. S3C, ESI†). Considering the absorbance maximum location, we chose a 405 nm laser diode (pulse frequency = 1.6 kHz and power = 1500 mW) installed on a commercially available laser engraver system NEJE DK-8-KZ. This system has many advantages over traditionally used femtosecond lasers in terms of availability, low cost, and the possibility of processing a significant area of material.[32,33]

The initial experiment was completed by performing laser scribing of the PET@UiO-66 surface using 9.9 mm s^{-1} scanning speed and 600 mW laser power. The laser path is schematically depicted in Fig. S5, ESI.† We observed the carbonisation of PET@UiO-66 in the place of the interaction with the laser beam spot. After laser ablation, PET@UiO-66 surface is converted to a black-coloured material (Fig. 2C). Surprisingly, the resulting black layer on the PET surface was homogeneous and exhibited considerable scratch resistance and stability during washing with water or organic solvents. A remarkably important finding for electronic applications is that the sheet resistance of the resulting material was significantly low (23.4 ± 1.3 Ω per square). Therefore, we decided to further optimise the laser treatment conditions by varying the irradiation time and laser power. The direct variation of parameters was complicated due to a rational search of the optimal regime. Thus, we conducted the optimisation process using the Nelder–Mead algorithm by varying the laser power (P) and beam penetration depth/speed (D) (Fig. 2B, Table S1;† a detailed description is provided in Section 4, ESI†). The sheet resistance is the main measure of the carbonisation efficiency, which also reflects the homogeneity of the resulting carbon layer. First, three random points were chosen to optimise the two laser parameters in a triangular parametric form (points 1–3 Fig. 2B). Subsequently, the highest-conductivity vertex of the triangle was identified and measured. Several operations of triangle contraction, expansion, and shrinkage were conducted. The identification of the lowest conductivity vertex points meaningfully decreased the electrical resistance. The design optimization allowed a decrease of the sheet resistance down to 10.4 ± 3.1 Ω per square. It represents one of the best results for laser-induced carbonization reported so far (Table S2, ESI†). Additionally, the homogeneity of the resulting layer was investigated by SEM (Fig. 2(C-1) and (C-2), S6A, ESI†), where a uniform carbon layer was distinctly visible. Moreover, laser patterning offers an important opportunity to design arbitrarily shaped conductive circuits (Fig. 2(C-3)). The SEM images of the poorly conductive composite demonstrated

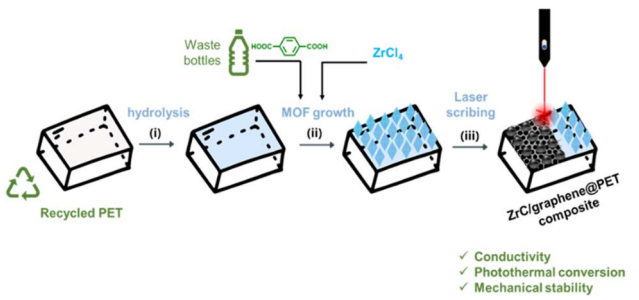

Fig. 1 Strategy for PET@LB-UiO-66 preparation from recycled PET: (i) PET hydrolysis, (ii) UiO-66 PET surface growth from waste PET bottle, and (iii) laser scribing process by 405 nm irradiation.

Published on 15 2565. Downloaded on 25/7/2567 1:05:24.

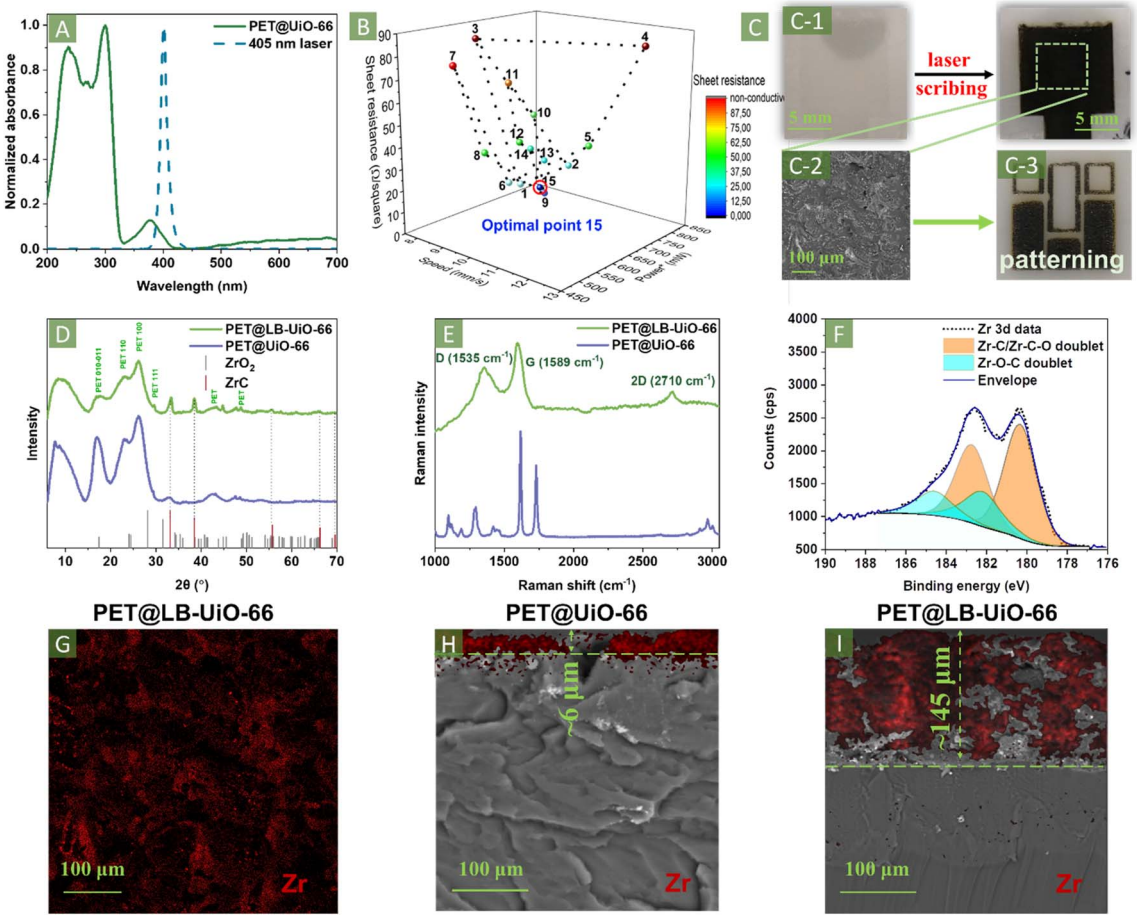

Fig. 2 (A) UV-vis spectrum of PET@UiO-66. (B) Optimization of PET@UiO-66 carbonization by the Nelder–Mead method. *Nominal laser power. (C) Material images before and after laser treatment: (C-1) a general view, (C-2) the SEM of PET@LB-UiO-66 after treatment under optimal conditions, and (C-3) optical image of the pattern (Logo Tomsk Polytechnic University) prepared by PET@UiO-66 laser scribing. Characterization of PET@LB-UiO-66: (D) XRD patterns, (E) Raman spectra, (F) Zr 3d XPS spectrum, and (G) EDX mapping of Zr from image on (C-2). Cross-sectional SEM-EDX images of (H) PET@UiO-66 and (I) PET@LB-UiO-66.

the formation of rough surfaces with agglomerates and non-uniformly distributed lumps (Fig. S6B, ESI†).

X-ray diffraction (XRD) analysis of the resulting composites characterised the prepared PET@LB-UiO-66 (using the optimised conditions *P*-49, *D*-26). The laser treatment led to the disappearance of UiO-66-characteristic peaks at 7.6° and 8.6° (Fig. 2D).[10] Instead, we observed new peaks at 33.2°, 38.4°, 55.7°, 66.2°, and 69.6°, which were identified as zirconium carbide.[49] The ZrC formation evidenced deep carbonisation, followed by the reduction of Zr clusters in the MOF structure by carbon. Surprisingly, despite the presence of atmospheric oxygen, we did not observe peaks associated with ZrO_2. It can be explained by the Zr reduction protected from environmental oxygen by the melted polymer layer. A comparison of the FTIR spectra of PET@UiO-66 and PET@LB-UiO-66 revealed the disappearance of UiO-66-related vibration bands (asymmetric and symmetric stretches of COO–Zr bonds at 1584 and 1397 cm^{-1}, respectively) after carbonisation, suggesting full conversion of the MOFs (Fig. S7, ESI†). Meanwhile, the characteristic bands of PET were still visible, confirming the formation of a composite between PET and carbonised UiO-66, similar to the previously reported conditions.[32,33]

These findings were corroborated by Raman spectroscopy. Laser treatment of PET@UiO-66 led to the loss of spectral features associated with the UiO-66 structure (Fig. 2E). Instead, in the PET@LB-UiO-66 Raman spectrum, we observed the characteristic peaks at 1362 and 1577 cm^{-1} assigned to the D and G peaks of graphene, in agreement with a previous report.[50] The characteristic fingerprint of 2D modes at 2670 cm^{-1} suggested the presence of few-layered graphene sheets impregnated in the polymer matrix.[51] Moreover, the relatively high intensity ratio ($I_D/I_G = 0.94$) indicates the high graphitization degree. It explains the low sheet resistance of the material.

The chemical composition of the resulting PET@LB-UiO-66 was studied using X-ray photoelectron spectroscopy (XPS) (Fig. 2F, S8 and S9 ESI†). Evaluation of the survey scan revealed changes in the surface concentrations of carbon, oxygen, and zirconium (Fig. S8A, ESI†). The C 1s peak deconvolution showed the same chemical state as that of PET@UiO-66. This result confirmed our assumption that graphene/ZrC is surrounded by

 This journal is © The Royal Society of Chemistry 2023

Published on 15 2565. Downloaded on 25/7/2567 1:05:24.

fused PET after the laser treatment (Fig. S8B, ESI†). Surprisingly, during initial analysis by XPS of PET@LB-UiO-66, Zr-related peaks were not observed (Fig. S8, ESI†). This is related to the penetration depth of XPS method with just a few nanometres and the distribution of Zr after laser scribing corresponding to cross-SEM with energy-dispersive X-ray (EDX) analysis (Fig. 2I). Therefore, we etched the surface using a monatomic Ar^+ depth-profiling technique, followed by XPS analysis (Fig. 2F and S9, ESI†). The presence of Zr 3d peaks at 180.3 and 182.7 eV infers the formation of zirconium carbide in the resulting material (Fig. 2F). Zr–O peaks are also observed in the Zr 3d spectra. We ruled out ZrO_2 formation by the XRD analysis discussed above. The Zr–O doublet formation is attributed to the partial substitution of C atoms by oxygen in the ZrC lattice.[52] Additionally, after laser scribing, the elemental composition of PET@UiO-66 changed only slightly in the C and Zr content according to the CHNS and inductively coupled plasma mass spectrometry (ICP-MS) (Table S3, ESI†).

The morphology of the resulting PET@LB-UiO-66 composite was elucidated using SEM (Fig. 2(C-2), G and I). Compared to pristine PET@UiO-66 (Fig. 2H and S3D–F, ESI†), drastic changes in surface morphology were distinctly observed. The microcrystalline MOF structure was transformed to a relatively smooth porous surface (Fig. 2(C-2)). Pore formation was promoted by laser-induced carbonisation owing to the generation of gas by-products, especially CO_2, after the decarboxylation of terephthalates.[32,33] EDX analysis of the treated surface revealed a homogenous distribution of Zr across the entire surface without significant particle agglomeration. Cross-sectional SEM imaging of PET@LB-UiO-66 was performed to determine the thickness of the carbonised layer. The thickness of the composite was significantly larger than that of UiO-66 (approximately 145 μm *vs.* approximately 6 μm), confirming our hypothesis regarding the active involvement of the PET melting process (Fig. 2H and I). Moreover, the formation of pores throughout the composite layer was distinctly observed. EDX analysis showed a relatively homogenous distribution of Zr in the vertical direction, suggesting drowning of solid particles during the melting of the PET matrix. At each stage of PET@LB-UiO-66 formation, we observed noticeable changes in morphology by SEM, profilometry, and water contact angle (WCA) measurements (see detailed description in Section 5 Fig. S10 and S11, ESI†). The laser scribing process of PET@UiO-66 led to the formation of a rough carbonaceous surface with visibly melted PET, impregnated carbon, and ZrC agglomerates.

To illustrate the importance of MOF coating homogeneity, we applied the optimised laser parameters to a sample prepared by drop-casting UiO-66 powder onto a PET plate. In this case, the non-homogeneously distributed UiO-66 crystals were not bound to the surface of PET (see details in Section 6, ESI†). Laser treatment of such composites under optimal conditions led to the carbonisation of UiO-66. However, the carbon layer was easily removed from PET by washing or mechanical bending of the composite, thus showing low mechanical stability of the carbon material (Fig. S12, ESI†). We assume that the low mechanical stability can be ascribed to the non-covalent binding of the UiO-66 layer to the PET surface. Therefore, in further experiments, we focused only on the optimised PET@LB-UiO-66 composite. In addition, we conducted control experiments to identify the role of surface UiO-66 in carbonisation. Thus, the treatment of pristine PET by laser (power 735 and 1500 mW) led to melting PET and negligible and uneven carbonisation (Fig. S13, ESI†). Nevertheless, according to SEM experiments for the determination of composite thickness, partial carbonisation of PET was also observed in PET@UiO-66, suggesting the critical role of UiO-66 as an analogue of the photosensitizer. We propose that carbonisation started from UiO-66, generating carbon material with impregnated ZrC clusters, which served as photothermal elements for the subsequent melting and carbonisation of PET matrix. The combination of these processes led to the formation of durable composites with enhanced properties.

Thus, the characterisation of PET@LB-UiO-66 demonstrated that laser-induced carbonisation led to the formation of a composite material composed of melted PET with impregnated graphene-like material and ZrC particles. Despite its obvious application as a conducting material, we hypothesised that the incorporation of ZrC would provide a considerable photothermal response.[53,54] Moreover, a high material conductivity should lead to a higher extinction coefficient and, hence, better light absorption.[55] For this reason, we assessed the photothermal properties of the resulting material to check its potential applicability in water steam generation and desalination technology, defogging, catalysis,[56] sensors,[57] bacterial killing,[58] deicing,[59] and photothermal electric power generation for wearable electronics, microelectronics,[60,61] and others.[62–65]

UV-vis spectroscopy analysis showed sufficient enhancement of PET@LB-UiO-66 absorbance, especially in the visible range (Fig. 3A), facilitating the interaction with light and significantly reducing the band gap energy in comparison with PET@UiO-66 (Fig. S14A and B, ESI†). For the analysis of the photothermal response, we measured the temperature after irradiation by LED at different wavelengths (455, 530, 660, 780, and 1055 nm; the power density of the LED is specified in ESI†) with subsequent temperature determination using a thermal infrared camera (Fig. 3B and C, S14C, ESI†). The temperature of the material increased rapidly, demonstrating its strong ability to convert visible and IR light into heat. After 100 s, the recorded temperatures stabilised at 65, 50, 71, 59, and 32 °C under 455, 530, 660, 780, and 1055 nm irradiation, respectively. Moreover, turning off the LED source led to a rapid decrease in the temperature, indicating excellent heat conductivity. Notably, in comparison with other related materials, PET@LB-UiO-66 (*P*-49, *D*-26) demonstrated the highest photothermal response considering the relatively low power of LED sources (Table S4, ESI†). Based on the possibility of using recycled PET as a support and terephthalic acid from waste PET bottles,[45] upcycled photothermal materials are highly competitive with other alternatives prepared from non-waste materials. We anticipate further studies using PET@LB-UiO-66 for desalination, vaporisation, and catalysis.[34,66]

In addition to photothermal performance, other factors such as stability, mechanical integrity, and cost should also be considered for practical applications.[66] The composite formed

Published on 15 2565. Downloaded on 25/7/2567 1:05:24.

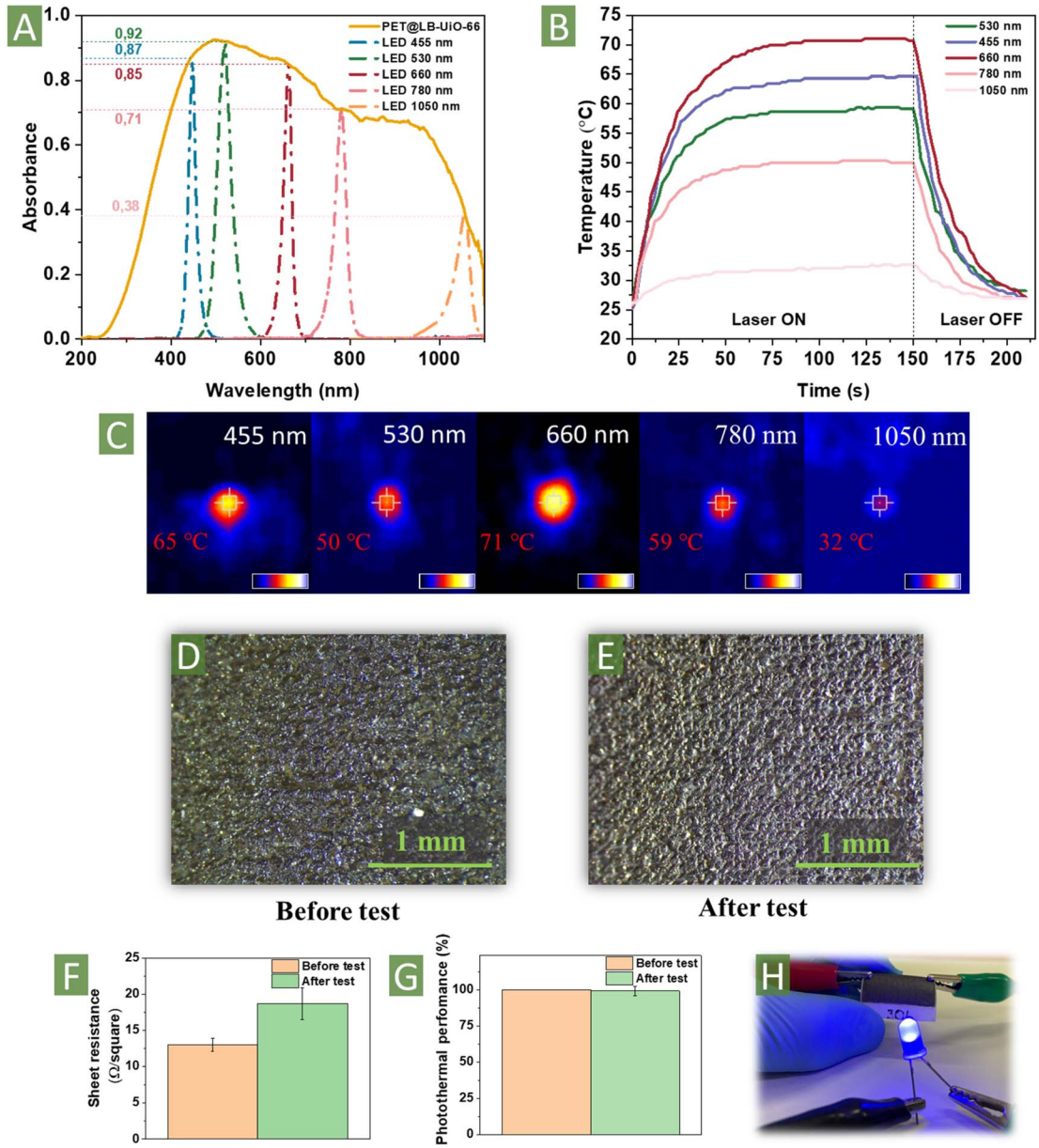

Fig. 3 (A) UV-vis spectrum of PET@LB-UiO-66 with spectra of LED sources. (B) Photothermal curves of PET@LB-UiO-66 acquired at 5 different wavelengths. (C) Images taken using a thermal camera during LED irradiation of PET@LB-UiO-66 at 5 different wavelengths. Optical microscopic photos: (D) before mechanical test and (E) after mechanical test. Comparison diagram of (F) sheet resistance and (G) photothermal performance before and after mechanical test. (H) Photo of bent PET@LB-UiO-66 used as a conductor to power LED.

from PET and impregnated graphene/ZrC should exhibit significant mechanical stability against abrasion and scratching. To evaluate the mechanical resilience of the material, we performed an abrasion test in a homemade vessel filled with sand for 24 h (Fig. S15, ESI†).[17] First of all, the optical microscopy analysis did not reveal a significant change in the surface morphology (Fig. 3D and E). No scratches or cracks were observed on the surface structure. For the applicability test, we recorded the sheet resistance and photothermal response after abrasive experiments (Fig. 3F and G). The sheet resistance slightly increased (up to $18.7 \pm 2.2\ \Omega$ per square), but it was still lower than that of the closest analogues carbonised ZIF-8/67 or polyimides (Table S2, ESI†). Thus, after abrasion, the material can be used as a conductor for LED sources or other circuits (Fig. 3H). At the same time, the sand treatment did not affect the photothermal response of PET@LB-UiO-66, suggesting the conservation of the layer structure. Additionally, we tested the solvent resistance of PET@LB-UiO-66 in different solvents, considering the stability of PET. Indeed, its stability in water and methanol has been proved by using it during the washing of the prepared materials. Treatment with more aggressive solvents led to the swelling of PET, followed by cracking of the

 This journal is © The Royal Society of Chemistry 2023

Published on 15 2565. Downloaded on 25/7/2567 1:05:24.

carbon surface, is presented in Fig. S16, ESI.† The developed methodology has a reasonable potential for further utilisation of PET on a large scale, considering the amount of waste PET.[67,68] For the scalability study, we repeated the procedure for the sample with a 5 cm^2 area (five times more than the common substrate). An optical image of the homogeneously carbonised materials is shown in Fig. S17, ESI,† suggesting that the developed approach can be successfully implemented on a larger scale.

In conclusion, we developed a novel approach for the smart upcycling of waste PET to create conductive materials with excellent photothermal properties through the surface-assisted growth of UiO-66 and subsequent laser-induced carbonisation. The combination of these procedures afforded durable and abrasion-resistant PET sheets coated with a graphene/zirconium carbide layer, providing enhanced electrical conductivity and photothermal properties. The excellent performance of the developed composite material and fabrication method made it possible to further apply waste PET in photothermal and electrochemical devices. We believe that the developed technology will open new avenues for the utilisation of waste polymers and their transformation into products of high added value.

Author Contributions

Dmitry Kogolev – investigation, data curation, visualization; Oleg Semyonov – investigation, Methodology, writing – original draft; Nadezhda Metalnikova – investigation, validation; Maxim Fatkullin – investigation, methodology; Raul D. Rodriguez – conceptualization, resources, writing – review & editing; Petr Slepicka – methodology, resources; Yusuke Yamauchi – resources, supervision, funding acquisition; Olga Guselnikova – methodology, conceptualization, writing – review & editing; Rabah Boukherroub – resources, funding acquisition, writing – review & editing; Pavel S. Postnikov – conceptualization, funding acquisition, supervision, writing – original draft.

Conflicts of interest

There are no conflicts to declare.

Acknowledgements

The authors thank the central laboratories of TPU (Analytical center) for the XPS measurements and Tomsk Regional Core Shared Research Facilities Center of National Research Tomsk State University for the SEM, ICP-MS and CHNS measurements. The research has been supported by the Russian-French project No. 075-15-2022-244 in the frame of PHC "Kholmogorov". R. B. acknowledges financial support from the CPER "Wavetech". This work was performed in part at the Queensland node of the Australian National Fabrication Facility, a company established under the National Collaborative Research Infrastructure Strategy to provide nano and microfabrication facilities for Australia's researchers.

References

1 S. S. Ali, T. Elsamahy, E. Koutra, M. Kornaros, M. El-Sheekh, E. A. Abdelkarim, D. Zhu and J. Sun, *Sci. Total Environ.*, 2021, **771**, 144719.
2 K. S. Khoo, L. Y. Ho, H. R. Lim, H. Y. Leong and K. W. Chew, *J. Hazard. Mater.*, 2021, **417**, 126108.
3 R. Zhang, X. Ma, X. Shen, Y. Zhai, T. Zhang, C. Ji and J. Hong, *J. Environ. Manage.*, 2020, **260**, 110062.
4 M. Khorram, A. Mousavi and N. Mehranbod, *J. Environ. Chem. Eng.*, 2017, **5**, 2366–2377.
5 V. Popescu, A. Muresan, O. Constandache, G. Lisa, E. I. Muresan, C. Munteanu and I. Sandu, *Ind. Eng. Chem. Res.*, 2014, **53**, 16652–16663.
6 O. Semyonov, D. Kogolev, G. Mamontov, E. Kolobova, A. Trelin, M. S. Yusubov, O. Guselnikova and P. S. Postnikov, *Chem. Eng. J.*, 2022, **431**, 133450.
7 W. Li, Z. Xie, S. Xue, H. Ye, M. Liu, W. Shi and Y. Liu, *Sep. Purif. Technol.*, 2021, **276**, 119435.
8 X. Tang, C. Din, S. Yu, Y. Liu, H. Luo, D. Zhang and S. Chen, *Chem. Eng. J.*, 2022, **446**, 137281.
9 W. P. R. Deleu, I. Stassen, D. Jonckheere, R. Ameloot and D. E. De Vos, *J. Mater. Chem. A*, 2016, **4**, 9519–9525.
10 O. Semyonov, S. Chaemchuen, A. Ivanov, F. Verpoort, Z. Kolska, M. Syrtanov, V. Svorcik, M. S. Yusubov, O. Lyutakov, O. Guselnikova and P. S. Postnikov, *Appl. Mater. Today*, 2021, **22**, 100910.
11 M. Shanmugam, C. Chuaicham, A. Augustin, K. Sasaki, P. J. J. Sagayaraj and K. Sekar, *New J. Chem.*, 2022, **46**, 15776–15794.
12 Q. Ren, H. Wang, X.-F. Lu, Y.-X. Tong, G.-R. Li, Q. Ren, H. Wang, X. Lu, Y. Tong and G. Li, *Adv. Sci.*, 2018, **5**, 1700515.
13 B. N. Bhadra, A. Vinu, C. Serre and S. H. Jhung, *Mater. Today*, 2019, **25**, 88–111.
14 M. Hao, M. Qiu, H. Yang, B. Hu and X. Wang, *Sci. Total Environ.*, 2021, **760**, 143333.
15 Q. Zhang, C. Xue, J. Wang, R. Huang, X. Hao and K. Li, *New Carbon Mater.*, 2021, **36**, 322–335.
16 D. Liu, W. Gu, L. Zhou, L. Wang, J. Zhang, Y. Liu and J. Lei, *Chem. Eng. J.*, 2022, **427**, 131503.
17 T. Wang, X. Cao, L. Jiao, T. Wang, X. Cao and L. Jiao, *Small*, 2021, **17**, 2004398.
18 S. Wu, J. Liu, H. Wang and H. Yan, *Int. J. Energy Res.*, 2019, **43**, 697–716.
19 J. Ren, Y. Huang, H. Zhu, B. Zhang, H. Zhu, S. Shen, G. Tan, F. Wu, H. He, S. Lan, X. Xia and Q. Liu, *Carbon Energy*, 2020, **2**, 176–202.
20 G. Chen, Z. Jiang, A. Li, X. Chen, Z. Ma and H. Song, *J. Mater. Chem. A*, 2021, **9**, 16805–16813.
21 J. Xu, Y. Jiang, X. Chen, Z. Tang, Y. Gao, M. Huang, Y. Wan, P. Cheng and G. Wang, *Mater. Today Nano*, 2022, **19**, 100234.
22 C. Geng, P. Wei, H. Chen, H. Liu, S. Zheng, H. Wang and Y. Xie, *Chem. Eng. J.*, 2021, **414**, 128878.
23 Y. Liu, Y. Sun and J. Zhang, *J. Mater. Chem. C*, 2017, **5**, 4286–4292.

Published on 15 2565. Downloaded on 25/7/2567 1:05:24.

24 F. Zheng, G. Xia, Y. Yang and Q. Chen, *Nanoscale*, 2015, **7**, 9637–9645.
25 J. Liu, D. Zhu, C. Guo, A. Vasileff, S.-Z. Qiao, J. L. Liu, D. D. Zhu, C. X. Guo, A. Vasileff, S.-Z. Qiao and -Z. S. Qiao, *Adv. Energy Mater.*, 2017, **7**, 1700518.
26 H. Jiang, S. Jin, C. Wang, R. Ma, Y. Song, M. Gao, X. Liu, A. Shen, G. J. Cheng and H. Deng, *J. Am. Chem. Soc.*, 2019, **141**, 5481–5489.
27 H. Jiang, L. Tong, H. Liu, J. Xu, S. Jin, C. Wang, X. Hu, L. Ye, H. Deng and G. J. Cheng, *Matter*, 2020, **2**, 1535–1549.
28 W. Zhang, R. Li, H. Zheng, J. Bao, Y. Tang, K. Zhou, W. Zhang, J. Bao, H. Zheng, K. Zhou, R. Li and Y. Tang, *Adv. Funct. Mater.*, 2021, **31**, 2009057.
29 Y.-J. Tang, H. Zheng, Y. Wang, W. Zhang, K. Zhou, Y. Tang, K. Zhou, H. Zheng, Y. Wang and W. Zhang, *Adv. Funct. Mater.*, 2021, **31**, 2102648.
30 A. Basu, K. Roy, N. Sharma, S. Nandi, R. Vaidhyanathan, S. Rane, C. Rode and S. Ogale, *ACS Appl. Mater. Interfaces*, 2016, **8**, 31841–31848.
31 D. Van Lam, M. Sohail, J. H. Kim, H. J. Lee, S. O. Han, J. Shin, D. Kim, H. Kim and S. M. Lee, *ACS Appl. Mater. Interfaces*, 2020, **12**, 39154–39162.
32 A. Lipovka, I. Petrov, M. Fatkullin, G. Murastov, A. Ivanov, N. E. Villa, S. Shchadenko, A. Averkiev, A. Chernova, F. Gubarev, M. Saqib, W. Sheng, J. J. Chen, O. Kanoun, I. Amin, R. D. Rodriguez and E. Sheremet, *Carbon*, 2022, **194**, 154–161.
33 R. D. Rodriguez, S. Shchadenko, G. Murastov, A. Lipovka, M. Fatkullin, I. Petrov, T.-H. Tran, A. Khalelov, M. Saqib, N. E. Villa, V. Bogoslovskiy, Y. Wang, C.-G. Hu, A. Zinovyev, W. Sheng, J.-J. Chen, I. Amin, E. Sheremet, R. D. Rodriguez, S. Shchadenko, G. Murastov, A. Lipovka, M. Fatkullin, I. Petrov, T. Tran, A. Khalelov, M. Saqib, N. E. Villa, V. Bogoslovskiy, A. Zinovyev, E. Sheremet, Y. Wang, C. Hu, J. Chen, W. Sheng and I. Amin, *Adv. Funct. Mater.*, 2021, **31**, 2008818.
34 H. Chen, S.-L. Wu, H.-L. Wang, Q.-Y. Wu and H.-C. Yang, *Adv. Energy Sustainability Res.*, 2021, **2**, 2000056.
35 B. Han, Y.-L. Zhang, Q.-D. Chen and H.-B. Sun, *Adv. Funct. Mater.*, 2018, **28**, 1802235.
36 R. D. Rodriguez, S. Shchadenko, G. Murastov, A. Lipovka, M. Fatkullin, I. Petrov, T. Tran, A. Khalelov, M. Saqib, N. E. Villa, V. Bogoslovskiy, Y. Wang, C. Hu, A. Zinovyev, W. Sheng, J. Chen, I. Amin and E. Sheremet, *Adv. Funct. Mater.*, 2021, **31**, 2008818.
37 Z. Kang, Y. Zhang and M. Zhou, *Chem. Eng. J.*, 2019, **368**, 223–234.
38 H. Ling, S. Liu, Z. Zheng and F. Yan, *Small Methods*, 2018, **2**, 1800070.
39 W. A. MacDonald, in *Large Area and Flexible Electronics*, Wiley-VCH Verlag GmbH & Co. KGaA, Weinheim, Germany, 2015, pp. 291–314.
40 R. D. Rodriguez, A. Khalelov, P. S. Postnikov, A. Lipovka, E. Dorozhko, I. Amin, G. v. Murastov, J.-J. Chen, W. Sheng, M. E. Trusova, M. M. Chehimi and E. Sheremet, *Mater. Horiz.*, 2020, **7**, 1030–1041.
41 G. Murastov, E. Bogatova, K. Brazovskiy, I. Amin, A. Lipovka, E. Dogadina, A. Cherepnyov, A. Ananyeva, E. Plotnikov, V. Ryabov, R. D. Rodriguez and E. Sheremet, *Biosens. Bioelectron.*, 2020, **166**, 112426.
42 A. Lipovka, I. Petrov, M. Fatkullin, G. Murastov, A. Ivanov, N. E. Villa, S. Shchadenko, A. Averkiev, A. Chernova, F. Gubarev, M. Saqib, W. Sheng, J.-J. Chen, O. Kanoun, I. Amin, R. D. Rodriguez and E. Sheremet, *Carbon*, 2022, **194**, 154–161.
43 J.-S. Kim, D. Ko, D.-J. Yoo, D. S. Jung, C. T. Yavuz, N.-I. Kim, I.-S. Choi, J. Y. Song and J. W. Choi, *Nano Lett.*, 2015, **15**, 2350–2357.
44 D. Y. Choi, H. W. Kang, H. J. Sung and S. S. Kim, *Nanoscale*, 2013, **5**, 977–983.
45 X. Dyosiba, J. Ren, N. M. Musyoka, H. W. Langmi, M. Mathe and M. S. Onyango, *Sustainable Mater. Technol.*, 2016, **10**, 10–13.
46 D. Van Lam, M. Sohail, V. T. Nguyen, Q. T. Ngo, A. Anto Jeffery, H. S. Choi, N. Jung, J. H. Kim, H. Kim and S. M. Lee, *Chem. Eng. J.*, 2021, **421**, 127731.
47 D. Van Lam, V.-T. Nguyen, E. Roh, Q.-T. Ngo, W. Choi, J.-H. Kim, H. Kim, H.-S. Choi, S.-M. Lee, D. V Lam, J. Kim, S. Lee, V. Nguyen, Q. Ngo, H. Choi, E. Roh, W. Choi and H. Kim, *Part. Part. Syst. Charact.*, 2021, **38**, 2100119.
48 D. Van Lam, D. T. Dung, J. H. Kim, H. Kim and S. M. Lee, *Chem. Eng. J.*, 2022, **437**, 135237.
49 J. X. Wang, D. W. Ni, S. M. Dong, G. Yang, Y. F. Gao, Y. M. Kan, X. W. Chen, Y. P. Cao and X. Y. Zhang, *RSC Adv.*, 2017, **7**, 22722–22727.
50 Y. Wu, Z. Huang, H. Jiang, C. Wang, Y. Zhou, W. Shen, H. Xu and H. Deng, *ACS Appl. Mater. Interfaces*, 2019, **11**, 44573–44581.
51 C. Li, L. Li, J. Li, X. Wu, L. Qi and W. Li, *Cellulose*, 2019, **26**, 1631–1640.
52 Q. Yan, B. Xin, Z. Chen and Y. Liu, *Mater. Today Commun.*, 2021, **28**, 102584.
53 R. Li, L. Zhang, L. Shi and P. Wang, *ACS Nano*, 2017, **11**, 3752–3759.
54 C. Song, X. Liu, M. Xu, D. Masi, Y. Wang, Y. Deng, M. Zhang, X. Qin, K. Feng, J. Yan, J. Leng, Z. Wang, Y. Xu, B. Yan, S. Jin, D. Xu, Z. Yin, D. Xiao and D. Ma, *ACS Catal.*, 2020, **10**, 10364–10374.
55 M. Xiong, X. Shan, C. Liu, L. Yang, M. Meng, Y. Di and Z. Gan, *Appl. Surf. Sci. Adv.*, 2021, **3**, 100050.
56 Q. Pan, S. Zhang, R. Li, Y. He and Y. Wang, *J. Mater. Chem. B*, 2019, **7**, 2948–2953.
57 S. Dash, J. de Ruiter and K. K. Varanasi, *Sci. Adv.*, 2018, **4**, eaat0127.
58 L. Zhu, T. Ding, M. Gao, C. K. N. Peh and G. W. Ho, *Adv. Energy Mater.*, 2019, **9**, 1900250.
59 P. Cheng, D. Wang and P. Schaaf, *Adv. Sustainable Syst.*, 2022, **6**, 2200115.
60 C. Abram, J. Shan, X. Yang, C. Yan, D. Steingart and Y. Ju, *ACS Appl. Energy Mater.*, 2019, **2**, 1319–1329.
61 B. Zhu, H. Kou, Z. Liu, Z. Wang, D. K. MacHaria, M. Zhu, B. Wu, X. Liu and Z. Chen, *ACS Appl. Mater. Interfaces*, 2019, **11**, 35005–35014.

 This journal is © The Royal Society of Chemistry 2023

62 X. Liu, X. Jin, L. Li, J. Wang, Y. Yang, Y. Cao and W. Wang, *J. Mater. Chem. A*, 2020, **8**, 12526–12537.
63 Q. Yan, B. Xin, Z. Chen and Y. Liu, *Mater. Today Commun.*, 2021, **29**, 102877.
64 L. Zhu, M. Gao, C. K. N. Peh and G. W. Ho, *Mater. Horiz.*, 2018, **5**, 323–343.
65 J. Chu, Y. Cai, C. Li, X. Wang, Q. Liu and M. He, *Waste Manage.*, 2021, **124**, 273–282.
66 S. Andreasi Bassi, D. Tonini, H. Saveyn and T. F. Astrup, *Environ. Sci. Technol.*, 2022, **56**, 501–511.
67 J. Chu, Y. Cai, C. Li, X. Wang, Q. Liu and M. He, *Waste Manage.*, 2021, **124**, 273–282.
68 S. Andreasi Bassi, D. Tonini, H. Saveyn and T. F. Astrup, *Environ. Sci. Technol.*, 2022, **56**, 501–511.

Published on 15 2565. Downloaded on 25/7/2567 1:05:24.